

Emergence of Hilbert Space Fragmentation in Ising Models with a Weak Transverse Field

Atsuki Yoshinaga,^{1,2,*} Hideaki Hakoshima,^{2,3} Takashi Imoto,² Yuichiro Matsuzaki,^{2,†} and Ryusuke Hamazaki^{4,‡}

¹*Department of Physics, The University of Tokyo,
5-1-5 Kashiwanoha, Kashiwa, Chiba 277-8574, Japan*

²*Research Center for Emerging Computing Technologies,
National Institute of Advanced Industrial Science and Technology (AIST),
Central2, 1-1-1 Umezono, Tsukuba, Ibaraki 305-8568, Japan*

³*Center for Quantum Information and Quantum Biology,
Osaka University, 1-2 Machikaneyama, Toyonaka 560-0043, Japan*

⁴*Nonequilibrium Quantum Statistical Mechanics RIKEN Hakubi Research Team,
RIKEN Cluster for Pioneering Research (CPR), RIKEN iTHEMS, Wako, Saitama 351-0198, Japan*

The transverse-field Ising model is one of the fundamental models in quantum many-body systems, yet a full understanding of its dynamics remains elusive in higher than one dimension. Here, we show for the first time the breakdown of ergodicity in d -dimensional Ising models with a weak transverse field in a prethermal regime. We demonstrate that novel Hilbert-space fragmentation occurs in the effective non-integrable model with $d \geq 2$ as a consequence of only one emergent global conservation law of the domain wall number. Our results indicate nontrivial initial-state dependence for non-equilibrium dynamics of the Ising models in a weak transverse field.

Introduction. — The transverse-field Ising model (TFIM) serves as a minimal model among quantum many-body systems [1, 2]. Despite its simplicity, the TFIM is quite difficult to investigate in higher-than-one dimensions because of its non-integrable nature. It is particularly important for foundation of quantum statistical mechanics to elucidate dynamical properties of the model. Indeed, its quantum thermalization has recently been investigated in relatively large systems [3–7]. For example, ergodicity in the ordered phase is controversial in the two-dimensional TFIM [3, 4, 8]. It was found that the model does not always thermalize in some quenches with numerical experiments [8] and that non-thermal eigenstates exist in a two-dimensional ladder system in the weak transverse-field limit [9].

The search for understanding quantum thermalization and the conditions behind it has been expanded substantially [10–22] in the recent decades because of the progress in experimental techniques [23–30]. One of the most important achievements is the eigenstate thermalization hypothesis (ETH) [10–12, 15, 31], which conjectures that all energy eigenstates are thermal and provides a sufficient condition for thermalization in isolated quantum systems. While the ETH has been confirmed numerically in various systems [15, 32–38], there is also growing interest in models violating the ETH. The emergence of non-thermal eigenstates has often been attributed to extensively many local conserved quantities due to, e.g., integrability [21, 39–42] and localization [43–47]. The Hilbert space fragmentation (HSF, or shattering) has recently attracted much attention as yet another mechanism of invalidating the ETH in non-integrable models [48–62]. In some models such as fractonic systems [63, 64], kinetic constraints impose restrictions on the dynamics [49–51] and create frozen regions which dynam-

ically divide the systems. This generates a fragmented structure of the Hilbert space with exponentially many nontrivial subspaces. In these cases, initial states cannot access the entire Hilbert space and fail to thermalize. For many previous models showing the HSF, the presence of at least two conserved quantities and the locality of the interaction were the origin of relevant kinetic constraints.

In this Letter, we show the emergence of non-ergodicity in a prethermal regime for Ising models with a weak transverse field on a hypercubic lattice in dimensions higher than one. In particular, by analytical calculations, we reveal for the first time that the effective model for the TFIM in the weak-transverse-field limit exhibits the HSF for $d \geq 2$. Notably, this effective model has only one global conserved quantity namely, the domain-wall (DW) conservation. The locality of the Hamiltonian and the DW conservation law leads to a kinetic constraint in the model (Fig. 1 (a)), and to the appearance of frozen regions. Due to the frozen regions, the Hilbert space is separated into exponentially many subspaces (Fig. 1 (b)). Consequently, the ETH breaks down and the effective model shows non-thermalizing behavior depending on the initial state. The emergence of frozen regions in our model is distinct from the ones in the previously studied models which require several conserved charges for exhibiting such frozen regions [49–51, 57]. For $d = 2$, we further demonstrate that rich dynamical properties are found in subspaces inside the DW sectors, including those found in non-integrable, integrable, and quantum many-body scarred systems [55, 65–67].

Model. — We consider the TFIM on a d -dimensional hypercubic lattice

$$\hat{H} = \hat{H}_{\text{DW}} + h_x \sum_i \hat{\sigma}_i^x, \text{ with } \hat{H}_{\text{DW}} := - \sum_{\langle i,j \rangle} \hat{\sigma}_i^z \hat{\sigma}_j^z, \quad (1)$$

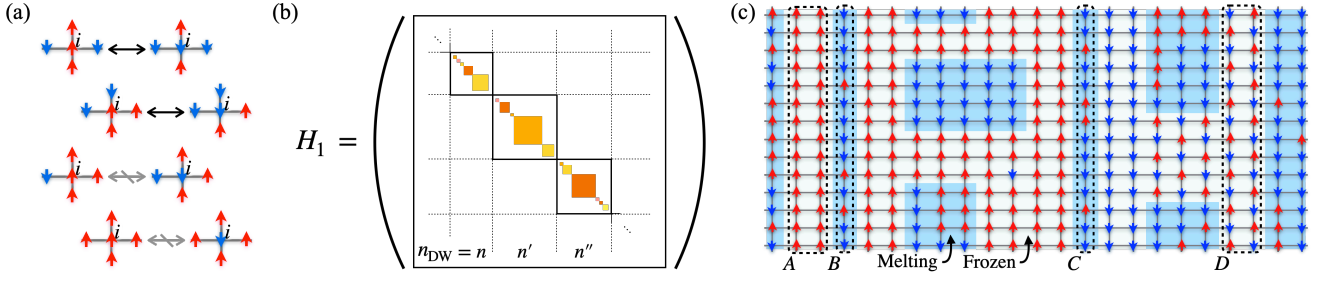


FIG. 1. (a) Schematic picture of the kinetic constraint arising from the projection operator \hat{Q}_i in the Hamiltonian Eq. (2) where we take the dimension d as two. Each spin at site i on a square lattice is flipped only when its two nearest neighbors are up and the other two spins are down. (b) Fragmented structure of the effective Hamiltonian. In addition to the block structure due to the conservation of the domain-wall number n_{DW} , the Hamiltonian matrix for an appropriate basis is further block diagonalized, namely fragmented. (c) An example of frozen regions (non-shaded) and melting regions (blue-shaded), where $d = 2$ and the periodic boundary condition is assumed. Red and blue arrows on each lattice site represent up and down spins in $\hat{\sigma}_i^z$ basis, respectively. The areas surrounded by dashed lines and labeled A and D exemplify prototypical spin configurations in frozen regions and those labeled B and C indicate one-dimensional melting regions which correspond to the PXP and XX models, respectively. Frozen regions percolate the system so that every spin in these regions is guaranteed to have at least three nearest-neighbor spins with the same sign.

where $\hat{\sigma}_i^\mu$ ($\mu = x, y, z$) denotes the Pauli spin operators at site i , $\langle i, j \rangle$ indicates that the sites i and j are neighboring, and h_x denotes the strength of the transverse field. While the DW number, i.e., the eigenvalues n_{DW} of $\sum_{\langle i, j \rangle} (1 - \hat{\sigma}_i^z \hat{\sigma}_j^z)/2$, is not conserved under the time evolution by \hat{H} for finite h_x , it is approximately conserved for a long time if h_x is sufficiently small [68]. Indeed, from a first-order perturbation theory, we obtain the following effective Hamiltonian [9, 69]:

$$\hat{H}_{\text{eff}} := \hat{H}_{\text{DW}} + h_x \hat{H}_1, \text{ with } \hat{H}_1 := \sum_i \hat{\sigma}_i^x \hat{Q}_i, \quad (2)$$

where the operator \hat{Q}_i projects all spin configurations onto the state space in which the sum of the z components of the $2 \times d$ spins surrounding the site i is zero (see Fig. 1 (a)). For example, the projector \hat{Q}_i for $d = 2$ is explicitly given by [70]

$$\hat{Q}_i := \frac{5}{8} - \frac{1}{16} \left(\sum_{j \in \text{ngbh}(i)} \hat{\sigma}_j^z \right)^2 + \frac{3}{8} \prod_{j \in \text{ngbh}(i)} \hat{\sigma}_j^z, \quad (3)$$

where $\text{ngbh}(i)$ denotes the nearest-neighbor sites of the site i . The effective Hamiltonian \hat{H}_{eff} approximates the dynamics of local observables governed by the original Hamiltonian (1) for a certain time scale that goes to infinity as $h_x \rightarrow 0$ [70–72].

Since \hat{H}_1 commutes with \hat{H}_{DW} , Hamiltonians \hat{H}_1 and \hat{H}_{eff} lead to the same dynamics when we specify a DW sector. Thus, we focus on the Hamiltonian \hat{H}_1 in the following. The Hamiltonian \hat{H}_1 is non-integrable as discussed later; it conserves the DW number and is block diagonalized accordingly. Apart from spatial symmetries, such as inversion, the Hamiltonian also has global chiral symmetry, i.e., \hat{H}_1 anti-commutes with $\prod_i \hat{\sigma}_i^\nu$ ($\nu = y, z$)

[73]. This symmetry produces non-zero energy eigenvalues in pairs with opposite signs. While the Hamiltonian also has global \mathbb{Z}_2 symmetry (i.e., \hat{H}_1 commutes with $\prod_i \hat{\sigma}_i^x$), we confirm that this symmetry is irrelevant for the emergence of HSF.

Hilbert space fragmentation. — We now demonstrate the Hilbert-space fragmentation of \hat{H}_1 in each sector characterized by the number of DWs (see Fig. 1 (b)). We first show that the kinetic constraint induced by \hat{Q}_i forms regions where the spin dynamics is frozen. More specifically, let us consider a product state $|F\rangle = \prod_{i \in \mathcal{F}} |s_i\rangle$ forming a sub-region \mathcal{F} on the entire lattice Λ , where $|s_i\rangle$ is one of the eigenstates of $\hat{\sigma}_i^z$. If $|F\rangle$ satisfies the following condition, we call \mathcal{F} a frozen region: $\hat{Q}_i(|F\rangle \otimes |M\rangle) = 0$ for $\forall i \in \mathcal{F}$ and any $|M\rangle$ defined on Λ/\mathcal{F} . The frozen regions remain unchanged under the time evolution by \hat{H}_1 (as well as \hat{H}_{eff}). Meanwhile, non-frozen regions, which we call melting regions, are isolated from one another and separated by frozen regions. Nontrivial dynamics occurs only in the melting regions. Below we focus on the case with $d = 2$ although most observations here hold for $d \geq 3$ too.

Figure 1 (c) exemplifies a possible spin configuration and associated frozen and melting regions. One simple example of the frozen region is a ladder-like region along the lattice with all spins aligning up in the z direction, percolating the system from one end to the other (the area A in Fig. 1 (c)). Another example is a wider region in which not all the spins are aligned in the same direction (the region between the areas B and C in Fig. 1 (c)) and surrounds some melting regions. A spin configuration in a frozen region can also exhibit a checker-board pattern (the area D in Fig. 1 (c)). In all of the cases, every spin is arranged in such a way that at least $(d+1)$ of its nearest-neighbor spins have the same direction, which

set the value of \hat{Q}_i to zero. Because this condition prohibits a frozen region from having corners under the periodic boundary conditions, we conjecture that all frozen regions percolate the system from one side to the other [70].

Because of the frozen regions, the Hilbert space has exponentially many subspaces. For example, a spin configuration having a frozen region cannot change into another spin configuration having a different frozen region by the Hamiltonian dynamics. This splits the Hilbert space into subspaces. Moreover, even when the arrangement of frozen regions is the same, there are many ways in which the DWs are spatially distributed over separated melting regions. Since the density of DW within each melting region is conserved over time, the Hilbert space is broken up into even smaller subspaces. Each subspace is therefore characterized by the configuration of the frozen regions and the spatial distribution of the DW density for melting regions.

The emergence of the dynamically fragmented subspaces suggests that the relaxation dynamics of the system strongly depends on the details of the initial state. When we take an initial state from one of the subspaces in a given DW sector and let it evolve, the state remains in this subspace. Let us consider, for example, two initial product states $|\psi_1\rangle$ and $|\psi_2\rangle$ shown in Fig. 2 (a), which are slightly different in their spin configurations but have the same energy in a DW sector. Figure 2 (b) shows the dynamics of the expectation value of the magnetization density from these two initial product states according to the effective Hamiltonian \hat{H}_{eff} . Throughout this Letter, we perform numerical calculations under the condition that the spins constituting the system are surrounded by fixed frozen spins pointing down. Due to the frozen region in the middle of the lattice, which emerges only in the state $|\psi_2\rangle$, the magnetization relaxes to substantially different values for the two initial conditions, which indicates ergodicity breaking. This example highlights that a frozen region covering a large area of the system can be converted into a melting region with a small change in the initial configuration in this model. Similar behavior can be also observed under the time evolution by \hat{H} with a weak h_x (see the Supplemental Material [70]).

The non-ergodicity due to the HSF in this model is deeply related to the violation of the ETH. The fragmented structure yields exponentially many non-thermal energy eigenstates. Simple examples of such non-thermal states are product frozen states, which correspond to the states in isolated subspaces with the dimension one. As detailed in Supplemental Material [70], we show that the number of frozen states increases exponentially in the system size, indicating the emergence of the HSF [62]. We note that Ref. [9] also finds a similar frozen state for an effective model of TFIM on a pseudo-one-dimensional ladder, but no HSF was discussed there. As another example, we find eigenstates which have spatially inhomogeneous

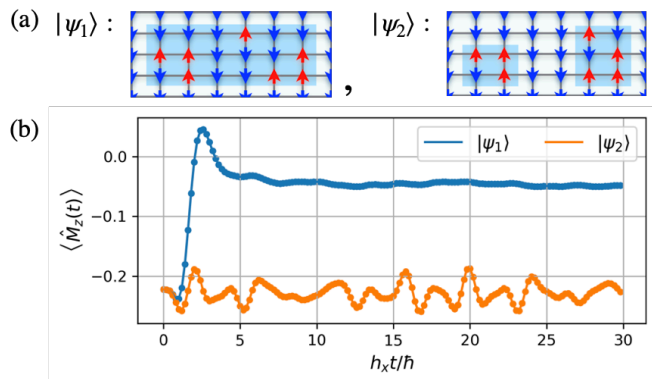


FIG. 2. (a) Spin configurations of the two initial states for a $N = 3 \times 6$ lattice. We assume that the system is surrounded by fixed spins pointing down. Regions with blue shades show melting ones. (b) Magnetization dynamics starting from the two initial product states. Time evolution of the expectation value $\langle \hat{M}_z(t) \rangle := \langle \psi(t) | (1/N) \sum_i \hat{\sigma}_i^z | \psi(t) \rangle$ shows that a slightly different initial condition results in substantially different stationary states.

DW density owing to frozen regions that act as a wall to separate different melting regions.

Figure 3 (a) shows the entanglement entropy of all the energy eigenstates of \hat{H}_1 in a fixed DW sector for a $N = 3 \times 6$ lattice [74]. We evaluate it by computing the von-Neumann entropy of the left half of the system. In generic systems obeying the ETH, eigenstate entanglement entropies are close to one another for close eigenenergies. In Fig. 3 (a), we demonstrate the violation of the ETH in this model, that is, a broad distribution of the entanglement entropy even for close eigenenergies and the presence of eigenstates with low entanglement. Due to the existence of frozen regions that divide the system into isolated parts, there are many eigenstates with zero bipartite entanglement [75].

Several remarks are in order. First, the kinetic constraint in \hat{H}_1 is associated with the conservation of the DW number alone. In particular, the model possesses frozen regions that dynamically divide the system and exhibits exponentially many frozen states. These properties are often found in the previously studied models [62] as a consequence of more than one conserved quantities [49–53, 57, 60]. Our finding here demonstrates that such nontrivial physics can occur even when there is only one apparent conserved quantity. Second, consequences of the percolation behavior of frozen regions depend on d . For $d = 2$, the system is always divided into isolated parts by frozen regions that percolate the system and act as walls. However, for $d > 2$, frozen regions do not always divide the system because their shape can be, e.g., a square prism which percolates only in one direction along the lattice. It is also worth mentioning that the Hamiltonian Eq. (2) does not yield many frozen regions and the resultant HSF for $d = 1$, while we show in fact

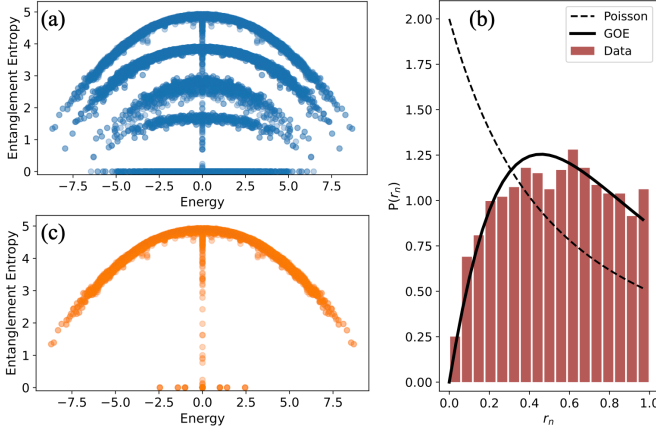


FIG. 3. (a) Entanglement entropy of all the energy eigenstates in a DW sector for a $N = 3 \times 6$ lattice. At its boundaries, the system is surrounded by fixed frozen spins pointing down. In all panels (a)–(c), we take $n_{\text{DW}} = 20$, for which $0 \leq n_{\text{DW}} \leq 36$. We find that the entanglement entropy exhibits a broad distribution even for a fixed energy, indicating the breakdown of the ETH in this DW sector. (b) Distribution of the consecutive energy-gap ratio r_n [76] for the subspace without frozen regions. The statistics is calculated after resolving the two spatial inversion symmetries along the x and y directions [77]. Dashed line shows the Poisson prediction $P_{\text{Poisson}}(r) = 2/(1+r)^2 \Theta(1-r)$ and the solid line shows the GOE prediction $P_{\text{GOE}}(r) = (27/4)(r+r^2)/(1+r+r^2)^{5/2} \Theta(1-r)$, where Θ is the Heaviside step function. The agreement between the result and the GOE prediction indicates the non-integrability of the system defined in this subspace. (c) Entanglement entropy of the energy eigenstates in the subspace without frozen regions (extracted from the panel (a)). Most of the eigenstates with close energies have similar values of entanglement entropy, in accordance with the ETH. Meanwhile, a small number of low-entangled eigenstates appear around specific values: $E = 0, \pm 1, \pm\sqrt{2}$ and $\pm\sqrt{6}$, which are regarded as quantum many-body scars [55, 65–67, 70].

it does for $d > 1$. Finally, eigenstates with frozen regions can be found in every DW sector as long as the system is sufficiently large. Thus, non-ergodic behavior can be found for initial states with any finite energy density with respect to the effective Hamiltonian \hat{H}_{eff} . This suggests that the original TFIM in a weak transverse field exhibits non-thermal behavior for long times at any energy scale for particular initial states.

Subspace properties. — Now we investigate properties of the fragmented subspaces of \hat{H}_1 . The dynamics for each subspace is observed only in the melting regions, being characterized by their shapes and their boundary conditions. Here we specifically consider the case for $d = 2$ and show that there are a rich variety of dynamics in some melting regions, including those found in non-integrable, integrable, and quantum many-body scarred systems.

The Hamiltonian \hat{H}_1 itself is presumably non-

integrable. To demonstrate this, let us choose a subspace having no frozen regions. In Fig. 3 (b), we perform the analysis of energy-level statistics for this subspace. We calculate the distribution of the consecutive energy-gap ratio $r_n = \min(\delta_n/\delta_{n-1}, \delta_{n-1}/\delta_n)$ with $\delta_n := E_{n+1} - E_n$, where E_n denotes the n th energy eigenvalue in the subspace [76]. The statistics of this ratio in Fig. 3 (b) shows a good agreement with that of the Gaussian Orthogonal Ensemble (GOE), indicating that this subspace as well as the entire \hat{H}_1 is non-integrable.

Additionally, in the subspace without frozen regions, we numerically find eigenstates with low entanglement in the bulk of the spectrum, which are regarded as quantum many-body scarred states [55, 65–67]. Figure 3 (c) demonstrates the presence of such states around $E = 0, \pm 1, \pm\sqrt{2}$ and $\pm\sqrt{6}$. The origin of these states cannot be attributed to frozen regions as they are excluded in this subspace. We find that some of them originate from specific local structures of the adjacency graph of the Hamiltonian [78, 79]; see the Supplemental Material for details [70].

Interestingly, we find that the one-dimensional PXP model and the XX model can be embedded as melting regions of the model \hat{H}_1 . First, let us discuss the emergent PXP model (see the area B in Fig. 1 (c)). In this one-dimensional region, all sites are adjacent to the frozen sites with up spins. Therefore, in this region, every spin can be flipped only when its two nearest neighbors are down due to the kinetic constraint. Hence, the system is effectively governed by

$$\hat{H}_B = \sum_{i \in B} \hat{\sigma}_i^x \frac{1}{4} (1 - \hat{\sigma}_{i+1}^z) (1 - \hat{\sigma}_{i-1}^z). \quad (4)$$

This is the one-dimensional PXP model, a well-known non-integrable model for hosting quantum many-body scars [66, 80–83]. This implies that one observes a long-lived oscillation of an observable in this one-dimensional region if we prepare an appropriate initial configuration. Second, let us briefly discuss the XX model (the area C in Fig. 1 (c)). In this region, the direction of the spin neighboring on the right side is opposite to that neighboring on the left side. We then find that the following Hamiltonian governs the dynamics in this region:

$$\hat{H}_C = \sum_{i \in C} \hat{\sigma}_i^x \frac{1}{2} (1 - \hat{\sigma}_{i+1}^z \hat{\sigma}_{i-1}^z). \quad (5)$$

This is the same as the effective Hamiltonian of the Ising chain in a weak transverse field [84] and is mappable to the XX chain [85], which is exactly solvable and thus ergodicity is broken due to the integrability. This implies that some subspaces become integrable when they only have a specific type of melting region.

Conclusion and outlook. — In this Letter we have rigorously demonstrated that the effective model obtained from the d -dimensional Ising model in a weak transverse

field on a hypercubic lattice exhibits the HSF for $d \geq 2$. In particular, the kinetic constraint, which is attributed to the emergent conservation of the DW number in this model, forms frozen regions that percolate the system. Consequently, each DW sector fractures into exponentially many isolated subspaces, leading to the violation of the ETH. We furthermore showed that some of the subspaces can be non-integrable, integrable, and even possess scarred eigenstates. Our results indicate that non-trivial initial-state dependence is observed for prethermal dynamics of the Ising models in a weak transverse field. Because the TFIM in two and three dimensions are experimentally realizable [5, 86–92], we believe that the model serves as a novel platform for observing the signatures of HSF, which is distinct from previous experiments that required, e.g., tilted potentials [93, 94]. We leave it for future work to investigate the robustness of transient non-ergodicity under long-range Ising interaction, which often arises in experiments. Finally, given that \hat{H}_{eff} is obtained in the weak-field limit of the TFIM, it is interesting to see how properties of the Ising model without the transverse field, such as (classical) integrability and finite-temperature phase transition, affect physics in our model.

Acknowledgments. — We are grateful to Naomichi Hatano for fruitful discussion and carefully reading the manuscript, and Rahul Nandkishore for insightful comments. A.Y. thanks Junichi Haruna for useful discussions. This work was supported by Leading Initiative for Excellent Young Researchers MEXT Japan, JST PRESTO (Grant No. JPMJPR1919) Japan, JST COI-NEXT program (JPMJPF2014), and MEXT Quantum Leap Flagship Program (MEXT Q-LEAP) Grant No. JPMXS0120319794.

* yoshi9d@iis.u-tokyo.ac.jp

† matsuzaki.yuichiro@aist.go.jp

‡ ryusuke.hamazaki@riken.jp

- [1] P. De Gennes, Collective motions of hydrogen bonds, *Solid State Commun.* **1**, 132 (1963).
- [2] R. Stinchcombe, Ising model in a transverse field. i. basic theory, *J. Phys. C* **6**, 2459 (1973).
- [3] K. R. Fratus and M. Srednicki, Eigenstate thermalization in systems with spontaneously broken symmetry, *Phys. Rev. E* **92**, 040103 (2015).
- [4] R. Mondaini, K. R. Fratus, M. Srednicki, and M. Rigol, Eigenstate thermalization in the two-dimensional transverse field ising model, *Phys. Rev. E* **93**, 032104 (2016).
- [5] E. Guardado-Sanchez, P. T. Brown, D. Mitra, T. Devakul, D. A. Huse, P. Schauß, and W. S. Bakr, Probing the quench dynamics of antiferromagnetic correlations in a 2d quantum ising spin system, *Phys. Rev. X* **8**, 021069 (2018).
- [6] M. Schmitt and M. Heyl, Quantum many-body dynamics in two dimensions with artificial neural networks,

- Phys. Rev. Lett.* **125**, 100503 (2020).
- [7] J. Richter, T. Heitmann, and R. Steinigeweg, Quantum quench dynamics in the transverse-field ising model: A numerical expansion in linked rectangular clusters, *SciPost Phys.* **9**, 031 (2020).
- [8] B. Blaß and H. Rieger, Test of quantum thermalization in the two-dimensional transverse-field ising model, *Sci. Rep.* **6**, 1 (2016).
- [9] B. van Voorden, J. Minář, and K. Schoutens, Quantum many-body scars in transverse field ising ladders and beyond, *Phys. Rev. B* **101**, 220305 (2020).
- [10] J. M. Deutsch, Quantum statistical mechanics in a closed system, *Phys. Rev. A* **43**, 2046 (1991).
- [11] M. Srednicki, Chaos and quantum thermalization, *Phys. Rev. E* **50**, 888 (1994).
- [12] H. Tasaki, From quantum dynamics to the canonical distribution: general picture and a rigorous example, *Phys. Rev. Lett.* **80**, 1373 (1998).
- [13] S. Goldstein, J. L. Lebowitz, R. Tumulka, and N. Zanghì, Canonical typicality, *Phys. Rev. Lett.* **96**, 050403 (2006).
- [14] S. Popescu, A. J. Short, and A. Winter, Entanglement and the foundations of statistical mechanics, *Nat. Phys.* **2**, 754 (2006).
- [15] M. Rigol, V. Dunjko, and M. Olshanii, Thermalization and its mechanism for generic isolated quantum systems, *Nature* **452**, 854 (2008).
- [16] P. Reimann, Foundation of statistical mechanics under experimentally realistic conditions, *Phys. Rev. Lett.* **101**, 190403 (2008).
- [17] S. Goldstein, J. L. Lebowitz, C. Mastrodonato, R. Tumulka, and N. Zanghì, Approach to thermal equilibrium of macroscopic quantum systems, *Phys. Rev. E* **81**, 011109 (2010).
- [18] M. Rigol and M. Srednicki, Alternatives to eigenstate thermalization, *Phys. Rev. Lett.* **108**, 110601 (2012).
- [19] C. Gogolin and J. Eisert, Equilibration, thermalisation, and the emergence of statistical mechanics in closed quantum systems, *Rep. Prog. Phys.* **79**, 056001 (2016).
- [20] H. Tasaki, Typicality of thermal equilibrium and thermalization in isolated macroscopic quantum systems, *Journal of Statistical Physics* **163**, 937 (2016).
- [21] F. H. Essler and M. Fagotti, Quench dynamics and relaxation in isolated integrable quantum spin chains, *J. Stat. Mech.* **2016**, 064002 (2016).
- [22] P. Reimann, Symmetry-prohibited thermalization after a quantum quench, *J. Stat. Mech.* **2021**, 103106 (2021).
- [23] T. Kinoshita, T. Wenger, and D. S. Weiss, A quantum newton's cradle, *Nature* **440**, 900 (2006).
- [24] A. Polkovnikov, K. Sengupta, A. Silva, and M. Vengalattore, Colloquium: Nonequilibrium dynamics of closed interacting quantum systems, *Rev. Mod. Phys.* **83**, 863 (2011).
- [25] M. Gring, M. Kuhnert, T. Langen, T. Kitagawa, B. Rauer, M. Schreitl, I. Mazets, D. A. Smith, E. Demler, and J. Schmiedmayer, Relaxation and prethermalization in an isolated quantum system, *Science* **337**, 1318 (2012).
- [26] M. Schreiber, S. S. Hodgman, P. Bordia, H. P. Lüschen, M. H. Fischer, R. Vosk, E. Altman, U. Schneider, and I. Bloch, Observation of many-body localization of interacting fermions in a quasirandom optical lattice, *Science* **349**, 842 (2015).
- [27] A. M. Kaufman, M. E. Tai, A. Lukin, M. Rispoli,

- R. Schittko, P. M. Preiss, and M. Greiner, Quantum thermalization through entanglement in an isolated many-body system, *Science* **353**, 794 (2016).
- [28] J. Smith, A. Lee, P. Richerme, B. Neyenhuis, P. W. Hess, P. Hauke, M. Heyl, D. A. Huse, and C. Monroe, Many-body localization in a quantum simulator with programmable random disorder, *Nat. Phys.* **12**, 907 (2016).
- [29] H. Labuhn, D. Barredo, S. Ravets, S. De Léséleuc, T. Macrì, T. Lahaye, and A. Browaeys, Tunable two-dimensional arrays of single rydberg atoms for realizing quantum ising models, *Nature* **534**, 667 (2016).
- [30] G. Kucsko, S. Choi, J. Choi, P. C. Maurer, H. Zhou, R. Landig, H. Sumiya, S. Onoda, J. Isoya, F. Jelezko, E. Demler, N. Y. Yao, and M. D. Lukin, Critical thermalization of a disordered dipolar spin system in diamond, *Phys. Rev. Lett.* **121**, 023601 (2018).
- [31] R. V. Jensen and R. Shankar, Statistical behavior in deterministic quantum systems with few degrees of freedom, *Phys. Rev. Lett.* **54**, 1879 (1985).
- [32] H. Kim, T. N. Ikeda, and D. A. Huse, Testing whether all eigenstates obey the eigenstate thermalization hypothesis, *Phys. Rev. E* **90**, 052105 (2014).
- [33] A. Khodja, R. Steinigeweg, and J. Gemmer, Relevance of the eigenstate thermalization hypothesis for thermal relaxation, *Phys. Rev. E* **91**, 012120 (2015).
- [34] L. D'Alessio, Y. Kafri, A. Polkovnikov, and M. Rigol, From quantum chaos and eigenstate thermalization to statistical mechanics and thermodynamics, *Advances in Physics* **65**, 239 (2016).
- [35] J. R. Garrison and T. Grover, Does a single eigenstate encode the full hamiltonian?, *Phys. Rev. X* **8**, 021026 (2018).
- [36] T. Yoshizawa, E. Iyoda, and T. Sagawa, Numerical large deviation analysis of the eigenstate thermalization hypothesis, *Phys. Rev. Lett.* **120**, 200604 (2018).
- [37] S. Sugimoto, R. Hamazaki, and M. Ueda, Test of the eigenstate thermalization hypothesis based on local random matrix theory, *Phys. Rev. Lett.* **126**, 120602 (2021).
- [38] S. Sugimoto, R. Hamazaki, and M. Ueda, Eigenstate thermalization in long-range interacting systems, *Phys. Rev. Lett.* **129**, 030602 (2022).
- [39] M. Rigol, V. Dunjko, V. Yurovsky, and M. Olshanii, Relaxation in a completely integrable many-body quantum system: an ab initio study of the dynamics of the highly excited states of 1d lattice hard-core bosons, *Phys. Rev. Lett.* **98**, 050405 (2007).
- [40] R. Steinigeweg, J. Herbrych, and P. Prelovšek, Eigenstate thermalization within isolated spin-chain systems, *Phys. Rev. E* **87**, 012118 (2013).
- [41] P. Calabrese, F. H. Essler, and G. Mussardo, Introduction to 'quantum integrability in out of equilibrium systems', *J. Stat. Mech.* **2016**, 064001 (2016).
- [42] L. Vidmar and M. Rigol, Generalized gibbs ensemble in integrable lattice models, *J. Stat. Mech.* **2016**, 064007 (2016).
- [43] A. Pal and D. A. Huse, Many-body localization phase transition, *Phys. Rev. B* **82**, 174411 (2010).
- [44] R. Nandkishore and D. A. Huse, Many-body localization and thermalization in quantum statistical mechanics, *Annu. Rev. Condens. Matter Phys.* **6**, 15 (2015).
- [45] M. Serbyn, Z. Papić, and D. A. Abanin, Local conservation laws and the structure of the many-body localized states, *Phys. Rev. Lett.* **111**, 127201 (2013).
- [46] D. A. Huse, R. Nandkishore, and V. Oganesyan, Phenomenology of fully many-body-localized systems, *Phys. Rev. B* **90**, 174202 (2014).
- [47] D. A. Abanin, E. Altman, I. Bloch, and M. Serbyn, Colloquium: Many-body localization, thermalization, and entanglement, *Rev. Mod. Phys.* **91**, 021001 (2019).
- [48] G. De Tomasi, D. Hetterich, P. Sala, and F. Pollmann, Dynamics of strongly interacting systems: From fock-space fragmentation to many-body localization, *Phys. Rev. B* **100**, 214313 (2019).
- [49] S. Moudgalya, A. Prem, R. Nandkishore, N. Regnault, and B. A. Bernevig, Thermalization and its absence within krylov subspaces of a constrained hamiltonian, *arXiv:1910.14048* (2019).
- [50] P. Sala, T. Rakovszky, R. Verresen, M. Knap, and F. Pollmann, Ergodicity breaking arising from hilbert space fragmentation in dipole-conserving hamiltonians, *Phys. Rev. X* **10**, 011047 (2020).
- [51] V. Khemani, M. Hermele, and R. Nandkishore, Localization from hilbert space shattering: From theory to physical realizations, *Phys. Rev. B* **101**, 174204 (2020).
- [52] Z.-C. Yang, F. Liu, A. V. Gorshkov, and T. Iadecola, Hilbert-space fragmentation from strict confinement, *Phys. Rev. Lett.* **124**, 207602 (2020).
- [53] T. Rakovszky, P. Sala, R. Verresen, M. Knap, and F. Pollmann, Statistical localization: From strong fragmentation to strong edge modes, *Phys. Rev. B* **101**, 125126 (2020).
- [54] H. Zhao, J. Vovrosh, F. Mintert, and J. Knolle, Quantum many-body scars in optical lattices, *Phys. Rev. Lett.* **124**, 160604 (2020).
- [55] M. Serbyn, D. A. Abanin, and Z. Papić, Quantum many-body scars and weak breaking of ergodicity, *Nat. Phys.* **17**, 675 (2021).
- [56] K. Lee, A. Pal, and H. J. Changlani, Frustration-induced emergent hilbert space fragmentation, *Phys. Rev. B* **103**, 235133 (2021).
- [57] A. Khudorozhkov, A. Tiwari, C. Chamon, and T. Neupert, Hilbert space fragmentation in a 2d quantum spin system with subsystem symmetries, *arXiv:2107.09690* (2021).
- [58] B. Mukherjee, D. Banerjee, K. Sengupta, and A. Sen, Minimal model for hilbert space fragmentation with local constraints, *Phys. Rev. B* **104**, 155117 (2021).
- [59] B. Buča, Out-of-time-ordered crystals and fragmentation, *Phys. Rev. Lett.* **128**, 100601 (2022).
- [60] A. Bastianello, U. Borla, and S. Moroz, Fragmentation and emergent integrable transport in the weakly tilted ising chain, *Phys. Rev. Lett.* **128**, 196601 (2022).
- [61] S. Moudgalya and O. I. Motrunich, Hilbert space fragmentation and commutant algebras, *Phys. Rev. X* **12**, 011050 (2022).
- [62] S. Moudgalya, B. A. Bernevig, and N. Regnault, Quantum many-body scars and hilbert space fragmentation: a review of exact results, *Rep. Prog. Phys.* **85**, 086501 (2022).
- [63] R. M. Nandkishore and M. Hermele, Fractons, *Annu. Rev. Condens. Matter Phys.* **10**, 295 (2019).
- [64] M. Pretko, X. Chen, and Y. You, Fracton phases of matter, *Int. J. Mod. Phys. A* **35**, 2030003 (2020).
- [65] S. Moudgalya, N. Regnault, and B. A. Bernevig, Entanglement of exact excited states of affleck-kennedy-lieb-tasaki models: Exact results, many-body scars, and vi-

- olation of the strong eigenstate thermalization hypothesis, *Phys. Rev. B* **98**, 235156 (2018).
- [66] C. J. Turner, A. A. Michailidis, D. A. Abanin, M. Serbyn, and Z. Papić, Weak ergodicity breaking from quantum many-body scars, *Nat. Phys.* **14**, 745 (2018).
- [67] Z. Papić, Weak ergodicity breaking through the lens of quantum entanglement, arXiv:2108.03460 (2021).
- [68] D. Abanin, W. De Roeck, W. W. Ho, and F. Huveneers, A rigorous theory of many-body prethermalization for periodically driven and closed quantum systems, *Commun. Math. Phys.* **354**, 809 (2017).
- [69] T. Close, F. Fadugba, S. C. Benjamin, J. Fitzsimons, and B. W. Lovett, Rapid and robust spin state amplification, *Phys. Rev. Lett.* **106**, 167204 (2011).
- [70] See Supplemental Material, which includes Refs. [95–100], for (i) the expression of \hat{Q}_i in arbitrary dimensions, (ii) numerical estimation of the timescale over which our effective model works well, (iii) a reason for the conjecture that frozen regions should percolate the system, (iv) analytic demonstration of the exponentially growing number of the subspaces, and (v) numerical and some exact results on the special eigenstates which are found in Fig. 3 (c).
- [71] Z. Gong, N. Yoshioka, N. Shibata, and R. Hamazaki, Error bounds for constrained dynamics in gapped quantum systems: Rigorous results and generalizations, *Phys. Rev. A* **101**, 052122 (2020).
- [72] Z. Gong, N. Yoshioka, N. Shibata, and R. Hamazaki, Universal error bound for constrained quantum dynamics, *Phys. Rev. Lett.* **124**, 210606 (2020).
- [73] The DW number conservation law and the chiral symmetry appear both in a periodic boundary condition and an open boundary condition.
- [74] When numerically diagonalizing the Hamiltonian for Figs. 3 (a) and (c), we added perturbative random longitudinal fields with average strength 10^{-5} . This is due to avoid ambiguity caused by exact degeneracy originating from unwanted symmetries such as inversion.
- [75] The distribution at $E = 0$ in Figs. 3 (a) and (c) still involves some ambiguity because of degeneracy of an exponentially large number of zero-energy states. This may imply that the degeneracy originates from not only the chiral symmetry and spatial inversion symmetry [101] but also some hidden ones, which are not broken by the additional longitudinal fields.
- [76] Y. Y. Atas, E. Bogomolny, O. Giraud, and G. Roux, Distribution of the ratio of consecutive level spacings in random matrix ensembles, *Phys. Rev. Lett.* **110**, 084101 (2013).
- [77] Note that the GOE distribution is obtained only after resolving apparent symmetries, whereas the Poisson-like distribution often appears when symmetries such as inversion are unresolved [4, 34, 102, 103].
- [78] J.-Y. Desaulles, A. Hudomal, C. J. Turner, and Z. Papić, Proposal for realizing quantum scars in the tilted 1d fermi-hubbard model, *Phys. Rev. Lett.* **126**, 210601 (2021).
- [79] F. M. Surace, M. Dalmonte, and A. Silva, Quantum local random networks and the statistical robustness of quantum scars, arXiv:2107.00884 (2021).
- [80] H. Bernien, S. Schwartz, A. Keesling, H. Levine, A. Omran, H. Pichler, S. Choi, A. S. Zibrov, M. Endres, M. Greiner, V. Vuletić, and M. D. Lukin, Probing many-body dynamics on a 51-atom quantum simulator, *Nature* **551**, 579 (2017).
- [81] C. J. Turner, A. A. Michailidis, D. A. Abanin, M. Serbyn, and Z. Papić, Quantum scarred eigenstates in a rydberg atom chain: Entanglement, breakdown of thermalization, and stability to perturbations, *Phys. Rev. B* **98**, 155134 (2018).
- [82] C.-J. Lin and O. I. Motrunich, Exact quantum many-body scar states in the rydberg-blockaded atom chain, *Phys. Rev. Lett.* **122**, 173401 (2019).
- [83] T. Iadecola, M. Schecter, and S. Xu, Quantum many-body scars from magnon condensation, *Phys. Rev. B* **100**, 184312 (2019).
- [84] J.-S. Lee and A. K. Khitrin, Stimulated wave of polarization in a one-dimensional ising chain, *Phys. Rev. A* **71**, 062338 (2005).
- [85] M. Ostmann, M. Marcuzzi, J. P. Garrahan, and I. Lesanovsky, Localization in spin chains with facilitation constraints and disordered interactions, *Phys. Rev. A* **99**, 060101 (2019).
- [86] M. W. Johnson, M. H. S. Amin, S. Gildert, T. Lanting, F. Hamze, N. Dickson, R. Harris, A. J. Berkley, J. Johansson, P. Bunyk, E. M. Chapple, C. Enderud, J. P. Hilton, K. Karimi, E. Ladizinsky, N. Ladizinsky, T. Oh, I. Perminov, C. Rich, M. C. Thom, E. Tolkacheva, C. J. S. Truncik, S. Uchaikin, J. Wang, B. Wilson, and G. Rose, Quantum annealing with manufactured spins, *Nature* **473**, 194 (2011).
- [87] J. G. Bohnet, B. C. Sawyer, J. W. Britton, M. L. Wall, A. M. Rey, M. Foss-Feig, and J. J. Bollinger, Quantum spin dynamics and entanglement generation with hundreds of trapped ions, *Science* **352**, 1297 (2016).
- [88] A. Kumar, T.-Y. Wu, F. Giraldo, and D. S. Weiss, Sorting ultracold atoms in a three-dimensional optical lattice in a realization of maxwell’s demon, *Nature* **561**, 83 (2018).
- [89] A. Browaeys and T. Lahaye, Many-body physics with individually controlled rydberg atoms, *Nat. Phys.* **16**, 132 (2020).
- [90] Y. Song, M. Kim, H. Hwang, W. Lee, and J. Ahn, Quantum simulation of cayley-tree ising hamiltonians with three-dimensional rydberg atoms, *Phys. Rev. Research* **3**, 013286 (2021).
- [91] S. Ebadi, T. T. Wang, H. Levine, A. Keesling, G. Semeghini, A. Omran, D. Bluvstein, R. Samajdar, H. Pichler, W. W. Ho, S. Choi, S. Sachdev, M. Greiner, V. Vuletić, and M. D. Lukin, Quantum phases of matter on a 256-atom programmable quantum simulator, *Nature* **595**, 227 (2021).
- [92] P. Scholl, M. Schuler, H. J. Williams, A. A. Eberharter, D. Barredo, K.-N. Schymik, V. Lienhard, L.-P. Henry, T. C. Lang, T. Lahaye, A. M. Läuchli, and A. Browaeys, Quantum simulation of 2d antiferromagnets with hundreds of rydberg atoms, *Nature* **595**, 233 (2021).
- [93] S. Scherg, T. Kohlert, P. Sala, F. Pollmann, B. H. Madhusudhana, I. Bloch, and M. Aidelsburger, Observing non-ergodicity due to kinetic constraints in tilted fermi-hubbard chains, *Nat. Commun* **12**, 4490 (2021).
- [94] T. Kohlert, S. Scherg, P. Sala, F. Pollmann, B. H. Madhusudhana, I. Bloch, and M. Aidelsburger, Experimental realization of fragmented models in tilted fermi-hubbard chains, arXiv:2106.15586 (2021).
- [95] S. Kirkpatrick and T. P. Eggarter, Localized states of a binary alloy, *Phys. Rev. B* **6**, 3598 (1972).

- [96] B. Sutherland, Localization of electronic wave functions due to local topology, *Phys. Rev. B* **34**, 5208 (1986).
- [97] R. Bueno and N. Hatano, Null-eigenvalue localization of quantum walks on complex networks, *Phys. Rev. Research* **2**, 033185 (2020).
- [98] C.-J. Lin, V. Calvera, and T. H. Hsieh, Quantum many-body scar states in two-dimensional rydberg atom arrays, *Phys. Rev. B* **101**, 220304 (2020).
- [99] H. Zhao, A. Smith, F. Mintert, and J. Knolle, Orthogonal quantum many-body scars, *Phys. Rev. Lett.* **127**, 150601 (2021).
- [100] O. Hart and R. Nandkishore, Hilbert space shattering and dynamical freezing in the quantum ising model, arXiv:2203.06188 [, *Phys. Rev. B* (to be published)] (2022).
- [101] M. Schecter and T. Iadecola, Many-body spectral reflection symmetry and protected infinite-temperature degeneracy, *Phys. Rev. B* **98**, 035139 (2018).
- [102] A. Gubin and L. F. Santos, Quantum chaos: An introduction via chains of interacting spins 1/2, *Am. J. Phys* **80**, 246 (2012).
- [103] R. Hamazaki, T. N. Ikeda, and M. Ueda, Generalized gibbs ensemble in a nonintegrable system with an extensive number of local symmetries, *Phys. Rev. E* **93**, 032116 (2016).

Supplemental Material for “Emergence of Hilbert Space Fragmentation in Ising Models with a Weak Transverse Field”

Atsuki Yoshinaga,^{1,2,*} Hideaki Hakoshima,^{2,3} Takashi Imoto,² Yuichiro Matsuzaki,^{2,†} and Ryusuke Hamazaki^{4,‡}

¹*Department of Physics, The University of Tokyo,
5-1-5 Kashiwanoha, Kashiwa, Chiba 277-8574, Japan*

²*Research Center for Emerging Computing Technologies,
National Institute of Advanced Industrial Science and Technology (AIST),
Central2, 1-1-1 Umezono, Tsukuba, Ibaraki 305-8568, Japan*

³*Center for Quantum Information and Quantum Biology,
Osaka University, 1-2 Machikaneyama, Toyonaka 560-0043, Japan*

⁴*Nonequilibrium Quantum Statistical Mechanics RIKEN Hakubi Research Team,
RIKEN Cluster for Pioneering Research (CPR), RIKEN iTHEMS, Wako, Saitama 351-0198, Japan*

EXPRESSION OF THE PROJECTOR \hat{Q}_i

In the main text, we introduce the projector \hat{Q}_i for the effective model and explain its meaning. Here, we discuss formal expression of \hat{Q}_i in arbitrary dimensions. Let us consider the system on a hypercubic lattice in d dimensions. The operator \hat{Q}_i projects all spin configurations onto the state space in which the sum of the z components of the $2 \times d$ spins surrounding the site i is zero. Then \hat{Q}_i can be formally given by

$$\hat{Q}_i = \prod_{n=1}^d \left((2n)^2 - \left(\sum_{j \in \text{ngbh}(i)} \hat{\sigma}_j^z \right)^2 \right) / (2n)^2. \quad (\text{S.1})$$

For $d = 2$, for example, this expression is reduced to

$$\hat{Q}_i = \frac{5}{8} - \frac{1}{16} \left(\sum_{j \in \text{ngbh}(i)} \hat{\sigma}_j^z \right)^2 + \frac{3}{8} \prod_{j \in \text{ngbh}(i)} \hat{\sigma}_j^z. \quad (\text{S.2})$$

and therefore the Hamiltonian $\hat{H}_1 = \sum_i \hat{\sigma}_i^x \hat{Q}_i$ described in the main text contains five-body interaction on the square lattice.

TIME EVOLUTION IN THE ISING MODEL IN A WEAK TRANSVERSE FIELD

The effective Hamiltonian \hat{H}_{eff} (as well as \hat{H}_1 , which we mainly focus in the main text) describes the prethermal dynamics of the transverse-field Ising model (TFIM) in a weak-transverse-field limit, as shown in Eq. (2) in the main text. Here we show the time evolution of observables according to the original Hamiltonian \hat{H} (Eq. (1) in the main text) with a finite transverse field h_x and compare it with the time evolution for \hat{H}_{eff} . Note that, in the other sections of this supplementary material, we perform numerical calculations on the system governed by \hat{H}_{eff} , not \hat{H} .

Let us consider two initial product states $|\tilde{\psi}_1\rangle$ and $|\tilde{\psi}_2\rangle$ in a system of size 3×4 , as shown in Fig. S1 (a).

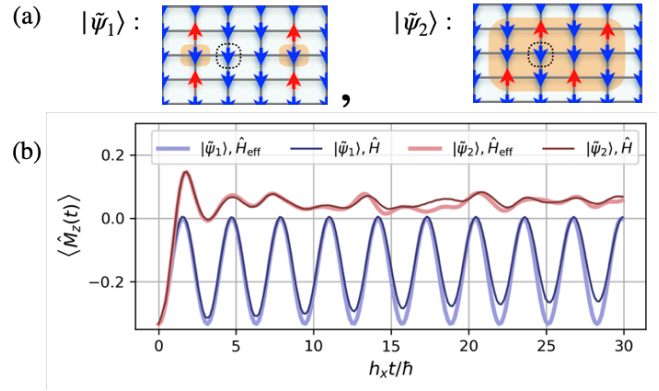


FIG. S1. (a) Spin configurations of the two initial product states for a $N = 3 \times 4$ lattice, where four spins are up and the others are down. Regions with orange shades show the melting regions with respect to the effective Hamiltonian \hat{H}_{eff} . Sites surrounded by broken lines indicate the location of the spin which we consider in Fig. S2 in this supplemental material. We assume that the system is surrounded by fixed spins pointing down. (b) Time evolution of the expectation value of the magnetization $\hat{M}_z := (1/N) \sum_i \hat{\sigma}_i^z$ starting from the two initial states. Solid thin lines describe dynamics according to the TFIM's Hamiltonian \hat{H} with $h_x = 0.3$ and solid thick lines show those of the effective Hamiltonian \hat{H}_{eff} .

These states have the same energy expectation value of \hat{H} . Throughout this supplementary material, we perform numerical calculations under the condition that the spins constituting the system are surrounded by fixed frozen spins pointing down. In Fig. S1 (b), we show dynamics from these two initial product states according to the two Hamiltonians \hat{H} and \hat{H}_{eff} , where we take $h_x = 0.3$. Specifically, we calculate the time evolution of the expectation value of the magnetization density. There is a good agreement between the dynamics with the original Hamiltonian and that with the effective Hamiltonian for a time range that we have adopted.

We also see from Fig. S1 (b) that the relaxation of the magnetization in the TFIM shows a strong dependence on the initial states. In the dynamics governed by \hat{H}_{eff} ,

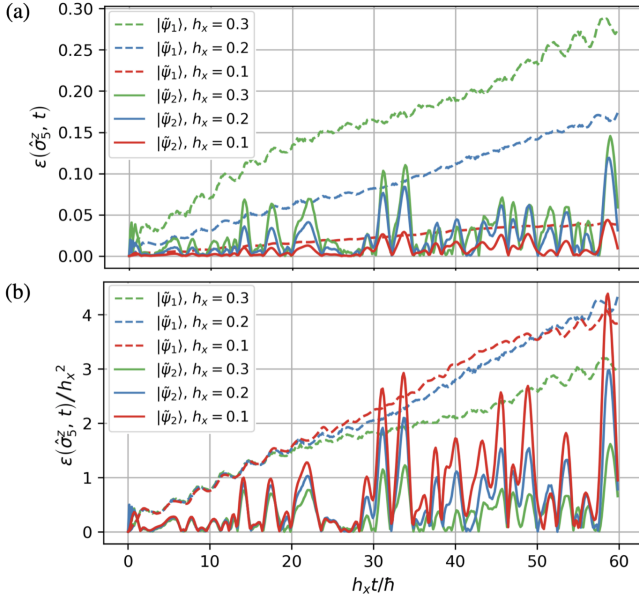


FIG. S2. Time evolution of the approximation error $\epsilon(\hat{\sigma}_i^z, t)$ starting from the two initial states $|\tilde{\psi}_1\rangle$ (three solid lines) and $|\tilde{\psi}_2\rangle$ (three broken lines) with different values of the transverse field, $h_x = 0.1, 0.2$ and 0.3 . We calculate the errors for the spin at the site $i = 5$ in the system (see Fig. S1 (a) in this supplemental material). The lower panel (b) shows the same data in the panel (a) but are rescaled by the square of the strength of the transverse field, i.e., $(h_x)^{-2}\epsilon(\hat{\sigma}_5^z, t)$.

there are only two melting sites and the other sites are frozen in $|\tilde{\psi}_1\rangle$ as shown in Fig. S1 (a). On the other hand, the entire system is melting in $|\tilde{\psi}_2\rangle$. This indicates that the two initial states belong to different subspaces in the fragmented Hilbert space of \hat{H}_{eff} . We can observe the emergence of the fragmented structure of the Hilbert space through the distinct behavior of the magnetization dynamics in the TFIM by preparing two different initial states.

As we decrease h_x to a smaller absolute value, the Hamiltonian \hat{H}_{eff} can approximate the dynamics of the TFIM for a longer time. To see this, we calculate the approximation error of the time evolution of a spin $\hat{\sigma}_i^z$,

$$\epsilon(\hat{\sigma}_i^z, t) := |\langle \hat{\sigma}_i^z(t) \rangle_{\text{TFIM}} - \langle \hat{\sigma}_i^z(t) \rangle|, \quad (\text{S.3})$$

where $\langle \hat{\sigma}_i^z(t) \rangle_{\text{TFIM}}$ and $\langle \hat{\sigma}_i^z(t) \rangle$ denote the expectation values which are evolved by the Hamiltonians \hat{H} and \hat{H}_{eff} , respectively. We observe that the error $\epsilon(\hat{\sigma}_5^z, t)$ grows more slowly as we decrease the transverse field h_x as shown in Fig. S2 (a). In Fig. S2 (b), we show the approximation errors that are rescaled by a power of the strength of the transverse field, i.e., $(h_x)^{-2}\epsilon(\hat{\sigma}_5^z, t)$. We find that the rescaled errors collapse clearly when we take $\alpha = 2$, especially for a relatively small time range. This implies that the approximation works well for a time scale

that grows with $\sim (1/h_x)^3$ as we decrease h_x .

FROZEN REGIONS AND PERCOLATION

We here discuss that the frozen regions should percolate the system by observing that they cannot have corners. As we explain in the main text, a frozen region \mathcal{F} satisfies the following condition: $\hat{Q}_i(|F\rangle \otimes |M\rangle) = 0$ for $\forall i \in \mathcal{F}$ and any $|M\rangle$ defined on Λ/\mathcal{F} , where $|F\rangle = \prod_{i \in \mathcal{F}} |s_i\rangle$ is a product state forming a sub-region \mathcal{F} on the entire lattice Λ and $|s_i\rangle$ denotes one of the eigenstates of $\hat{\sigma}_i^z$. We argue that a region with corners, e.g., \mathcal{G} in Fig. S3, cannot be a frozen region. Let us focus on a corner spin at site i belonging to \mathcal{G} and consider its $2d$ adjacent sites. Among such adjacent sites, we assume that j_{d+1}, \dots, j_{2d} belong to \mathcal{G} while j_1, \dots, j_d do not belong to \mathcal{G} . If \mathcal{G} were a frozen region, the spins on $i, j_{d+1}, \dots, j_{2d}$ would point some fixed directions (up or down in the z direction), whereas j_1, \dots, j_d would belong to a melting region. Since the melting region is described by a superposition of various different spin configurations under the time evolution by \hat{H}_{eff} , the spin directions at every site j_k ($1 \leq k \leq d$) can be opposite to those at the corresponding sites j_{k+d} in one of the spin configurations, and the sum of the z components of all adjacent spins can be zero in this particular case. This means that the spin at site i can flip with a finite probability. This contradicts our assumption that \mathcal{G} is frozen. In conclusion, the above discussion indicates that if a region has corners surrounded by melting regions, the region generally cannot be frozen. In other words, due to this condition, any frozen region should percolate the system. For a system with $d = 2$ under the periodic boundary conditions, they wrap around the torus in the x or y direction.

Fig. S3 (c) illustrates an example of melting of spins on a region with corners. Even if all spins are aligned in the same direction in a certain region, the spin flip will occur from the corners of the region, and the spin-flip region gradually spreads.

EXPONENTIALLY MANY FROZEN STATES

In this section, we demonstrate that the number of fragmented subspaces increases exponentially in the system size. In the main text, we show that this system has not only frozen states but also subspaces with both frozen and melting regions, and that it leads to the fragmented Hilbert space. Here, we show that the number of frozen states as well as the subspaces with both frozen and melting regions increases exponentially. First, we illustrate one way of constructing many frozen states for a given DW number $n_{\text{DW}} = \alpha_{\text{tot}} N$, where α_{tot} denotes DW density with $0 < \alpha_{\text{tot}} < 2$, and N denotes the system size with $N \gg 1$. For brevity we consider a two-dimensional

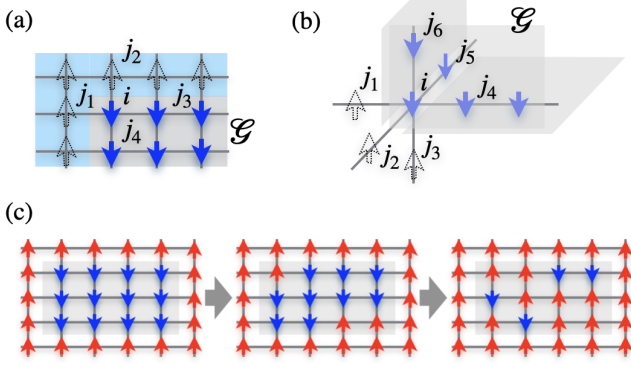


FIG. S3. Spins around a corner of a region \mathcal{G} (gray shaded) (a) for $d = 2$ and (b) for $d = 3$ (panel (b)). The spin at the corner site i of \mathcal{G} , whose d adjacent sites belong to \mathcal{G} and the other d adjacent sites do not, can always be flipped when the adjacent spins outside of \mathcal{G} have specific directions. (c) Example of melting of an aligned region with corners. Even if all spins are aligned down in a region with corners (gray-shaded region), given that the region is surrounded by up spins, the spin flip will occur from the corners of the region, and the spin-flip region gradually spread, and generally all sites within this region will melt.

system with its total sites $N = L^2$ and assume $L/l \in \mathbb{N}$ for an odd integer $l = \mathcal{O}(1)$ in the following. First, we divide the system into N/l^2 subregions as we show in the rightmost figure in Fig. S4. Second, we consider embedding either spin configuration (p1) or (p2) into each divided subregion, where (p1) denotes an example of an almost staggered configuration and (p2) denotes an example of an all-up configuration as shown in Fig. S4. The DW density for each configuration (p1) and (p2) is given by $\alpha_{p1} = 2 - (8l - 10)/l^2$ and $\alpha_{p2} = 0$. In this case, the total number of all possible combinations of the embedding is estimated as $(N/l^2)! / (k!(N/l^2 - k)!) = \exp[\mathcal{O}(N)]$, where $k = \mathcal{O}(N)$ satisfies $\alpha_{\text{tot}} N = \alpha_{p1} k l^2 + \alpha_{p2} (N - k l^2)$. This indicates that the number of frozen states constructed in the above procedure increases exponentially in the system size N in any DW sectors with finite DW densities.

We extend the above discussion to the case of the subspace with both frozen and melting regions. The configurations (p1) and (p2) should be replaced following the discussion below. As in (p1) and (p2), we consider the configurations that consist of the inner part where each spin can point up or down and the outer frozen part surrounding it where the spins always point up. Here, it is guaranteed that the outer spins are freezing because the spins always point up on the edges of the adjacent subregions in our configuration. Then, if we want to create subspaces that are partially frozen and partially melting, we can replace (p1) or (p2) with another configuration in which the inner parts are melting.

In addition, we can easily extend the above construction to the three dimensional case. Instead of a square,

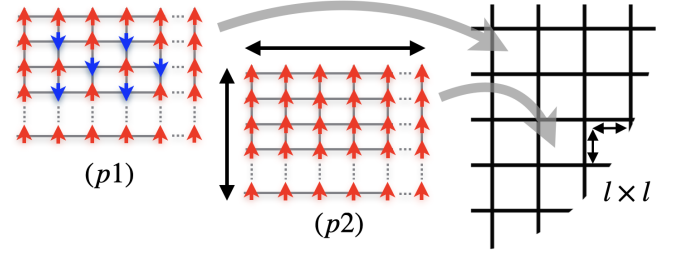


FIG. S4. Construction of frozen states. (p1) and (p2) describe possible spin configurations for subsystems with $l \times l$ sites. We can construct frozen states by embedding either spin configurations (p1) [almost staggered configuration] or (p2) [all-up configuration] as the subregions of the total system in the rightmost figure, which is divided into separated subregions.

we can consider a cube whose surface consists of frozen up spins. For the inner parts, the same discussion as the two dimensional case can be done for the three dimensional case.

Finally, it should be noted that the configurations illustrated here are just possible examples, and that there are indeed far more diverse and numerous possible subspaces associated with configurations of frozen or melting regions.

ATYPICAL STATES IN THE SUBSPACE WITHOUT FROZEN REGIONS

In Fig. 3 (c) in the main text, we find that some eigenstates show zero bipartite entanglement even in the subspace without frozen regions. They have specific energies $E = 0, \pm 1, \pm\sqrt{2}$, and $\pm\sqrt{6}$ in our calculation in Fig. 3 (c). Such low-entangled eigenstates in the middle of the energy spectrum of non-integrable models have been attracting much attention recently and are referred to as quantum many-body scars [1–4]. Here we discuss the origin of these states. We specifically focus on the eigenstates with non-zero energies. For the energy eigenstates with zero energy, the analysis is difficult due to the large degeneracy, and therefore we leave investigation of these states for future work.

We find that the origin of some atypical states in Fig. 3 (c) in the main text is well captured by an adjacency graph of the Hamiltonian \hat{H}_1 , where the nodes represent the computational-basis states and the edges between the nodes describe the connections by the off-diagonal elements of the Hamiltonian (see Fig. S5). The atypical eigenstates correspond to wave functions that are localized on part of the adjacency graph, which we call localized energy eigenstates. We use the word of “localized energy eigenstate” in order to refer to an eigenstate composed of superpositions of a small number of computational basis states. Similar states with low en-

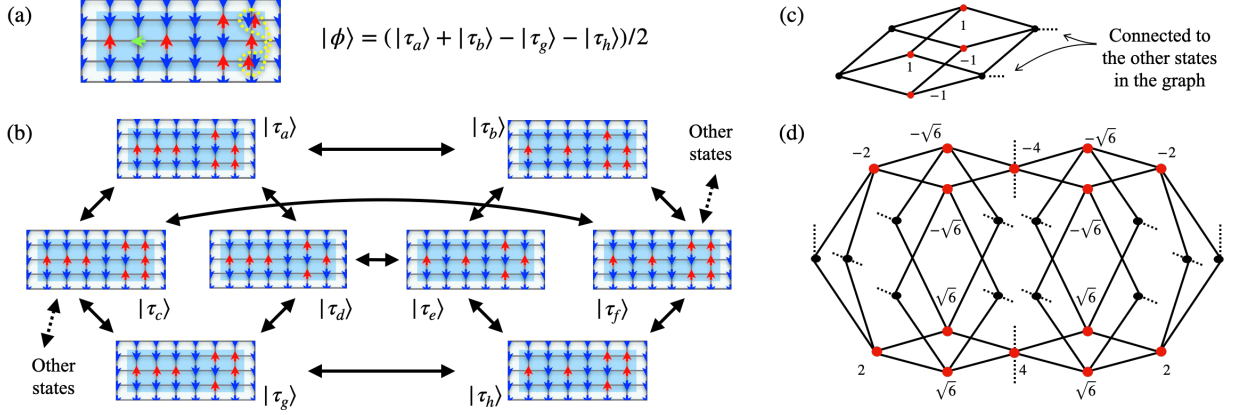


FIG. S5. (a) Schematic picture of a zero-entanglement eigenstate $|\phi\rangle$ with the energy 1 in Fig. 3 (c) in the main text. Red and blue arrows on each lattice site represent up and down spins in $\hat{\sigma}_i^z$ basis, respectively. The green arrow represents the spin pointing to the x direction, i.e., the eigenstate of $\hat{\sigma}_i^x$ with the eigenvalue $+1$, and the spins surrounded by the yellow broken line form a spin-singlet state. (b) Schematic picture of local structure of the adjacency graph that generates the localized eigenstate $|\phi\rangle$. Black arrows indicate that the two spin configurations are connected by the off-diagonal elements of the Hamiltonian matrix. The states $|\tau_c\rangle$ and $|\tau_f\rangle$ are connected with other states in the bulk of the graph which are not shown here. (c, d) Examples of local graph structures that give rise to localized energy eigenstates. The graph in (c) describes the same graph structure as in (b). Red nodes represent the basis with non-zero amplitudes in a localized energy eigenstate with the eigenenergy $E = 1$ [$E = \sqrt{6}$] for (c) [(d)], and the numbers associated with the red nodes represent the actual values of the amplitude (before normalization).

tanglement which are associated with the structure of the adjacency graph have been discussed recently [5, 6]. Localized eigenstates in a similar setting are also studied for example in Refs. [7–9], where the graph in these context is defined on the real space.

Figure S5 (a) describes one of the localized eigenstates with $E = 1$. In this case, the state $|\phi\rangle$ in Fig. S5 (a) is identified as a superposition of four computational basis states. These basis states are connected to other states in the subspace on the adjacency graph. Part of the graph is described in Fig. S5 (b). In general, when \hat{H}_1 acts on one of the basis states, it becomes a superposition of several basis states. However, the state $|\phi\rangle$ is still localized on the graph due to a destructive interference on the other nodes, which allows $|\phi\rangle$ to be an eigenstate of \hat{H}_1 . Such eigenstates that are expanded by only a few number of basis states have only limited amount of entanglement and even show zero entanglement entropy when the bipartite cut is set suitably.

There are various types of local structures of the adjacency graph which allow for localized eigenstates. Figure S5 (c) and (d) show two examples of such structures. Note that the graph in Fig. S5 (b) represents the same state described by the panel in Fig. S5 (c). As is exemplified by this state, localized eigenstates appear when some part of the adjacency graph of the Hamiltonian has a structure that induces the destructive interference. Indeed, low-entangled eigenstates with $E = \pm 1, \pm\sqrt{2}$, and $\pm\sqrt{6}$ (and a part of the eigenstates for $E = 0$) in Fig. 3 (c) in the main text are identified as localized eigenstates on the adjacency graph with local structures described

either in Fig. S5 (c) or (d).

Finally, from numerical simulations, we observe oscillatory behavior associated with the localized eigenstates, which is a typical signature of quantum many-body scarred systems [1, 10–13]. In Fig. S6 (b), we show dynamics of the magnetization starting from two initial states in Fig. S6 (a). Specifically, we calculate the time evolution of the expectation value of the magnetization density for a system surrounded by fixed down spins. For

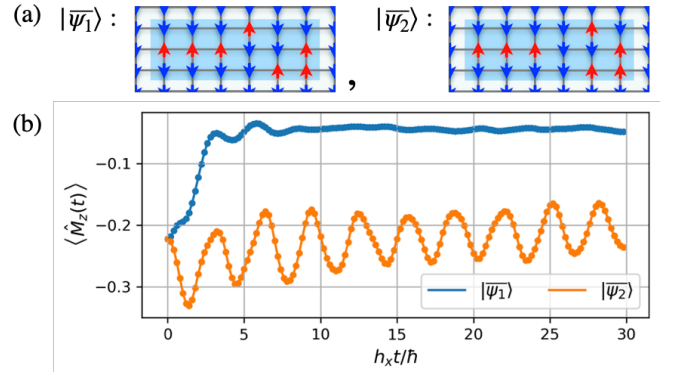


FIG. S6. (a) Spin configurations of the two initial states. We take the fixed boundary condition surrounded by down spins. Note that the state $|\psi_2\rangle$ corresponds to the state $|\tau_a\rangle$ in Fig. S5 (b). (b) Magnetization dynamics for two initial product states according to \hat{H}_1 . We numerically calculate the evolution of the expectation value of the magnetization $\hat{M}_z := (1/N) \sum_i \hat{\sigma}_i^z$ for a $N = 3 \times 6$ lattice.

the initial state $|\overline{\psi}_2\rangle$ in Fig. S6 (a), namely the state $|\tau_a\rangle$ in Fig. S5 (b), which has a large overlap with the state $|\phi\rangle$, we observe a long time oscillation. On the other hand, for typical initial states including $|\overline{\psi}_1\rangle$, the system rapidly relaxes to a steady state. This result, combined with the other results in the main text and supplementary materials, suggests that our model possesses various types of quantum many-body scar states in some subspaces such as those mappable to the PXP model [1, 11, 14, 15] and those with localized states.

Note added. — While we are revising our manuscript during the review process, a paper discussing a similar proof in appeared on arXiv [16]. However, it is worth mentioning that our proof in (added for supplementing our claim in the first version of our manuscript) focuses on the number of subspaces in each DW sector while the proof in Ref. [16] focuses on that of the entire Hilbert space.

* yoshi9d@iis.u-tokyo.ac.jp

† matsuzaki.yuichiro@aist.go.jp

‡ ryusuke.hamazaki@riken.jp

- [1] C. J. Turner, A. A. Michailidis, D. A. Abanin, M. Serbyn, and Z. Papić, Weak ergodicity breaking from quantum many-body scars, *Nat. Phys.* **14**, 745 (2018).
- [2] S. Moudgalya, N. Regnault, and B. A. Bernevig, Entanglement of exact excited states of affleck-kennedy-lieb-tasaki models: Exact results, many-body scars, and violation of the strong eigenstate thermalization hypothesis, *Phys. Rev. B* **98**, 235156 (2018).
- [3] M. Serbyn, D. A. Abanin, and Z. Papić, Quantum many-body scars and weak breaking of ergodicity, *Nat. Phys.* **17**, 675 (2021).
- [4] Z. Papić, Weak ergodicity breaking through the lens of quantum entanglement, arXiv:2108.03460 (2021).

- [5] J.-Y. Desaulles, A. Hudomal, C. J. Turner, and Z. Papić, Proposal for realizing quantum scars in the tilted 1d fermi-hubbard model, *Phys. Rev. Lett.* **126**, 210601 (2021).
- [6] F. M. Surace, M. Dalmonte, and A. Silva, Quantum local random networks and the statistical robustness of quantum scars, arXiv:2107.00884 (2021).
- [7] S. Kirkpatrick and T. P. Eggarter, Localized states of a binary alloy, *Phys. Rev. B* **6**, 3598 (1972).
- [8] B. Sutherland, Localization of electronic wave functions due to local topology, *Phys. Rev. B* **34**, 5208 (1986).
- [9] R. Bueno and N. Hatano, Null-eigenvalue localization of quantum walks on complex networks, *Phys. Rev. Research* **2**, 033185 (2020).
- [10] H. Bernien, S. Schwartz, A. Keesling, H. Levine, A. Omran, H. Pichler, S. Choi, A. S. Zibrov, M. Endres, M. Greiner, V. Vuletić, and M. D. Lukin, Probing many-body dynamics on a 51-atom quantum simulator, *Nature* **551**, 579 (2017).
- [11] C. J. Turner, A. A. Michailidis, D. A. Abanin, M. Serbyn, and Z. Papić, Quantum scarred eigenstates in a rydberg atom chain: Entanglement, breakdown of thermalization, and stability to perturbations, *Phys. Rev. B* **98**, 155134 (2018).
- [12] C.-J. Lin, V. Calvera, and T. H. Hsieh, Quantum many-body scar states in two-dimensional rydberg atom arrays, *Phys. Rev. B* **101**, 220304 (2020).
- [13] H. Zhao, A. Smith, F. Mintert, and J. Knolle, Orthogonal quantum many-body scars, *Phys. Rev. Lett.* **127**, 150601 (2021).
- [14] C.-J. Lin and O. I. Motrunich, Exact quantum many-body scar states in the rydberg-blockaded atom chain, *Phys. Rev. Lett.* **122**, 173401 (2019).
- [15] T. Iadecola, M. Schecter, and S. Xu, Quantum many-body scars from magnon condensation, *Phys. Rev. B* **100**, 184312 (2019).
- [16] O. Hart and R. Nandkishore, Hilbert space shattering and dynamical freezing in the quantum ising model, arXiv:2203.06188 [, *Phys. Rev. B* (to be published)] (2022).